ISSN 1063-7788, Physics of Atomic Nuclei, 2011, Vol. 74, No. 7, pp. 984–1000. © Pleiades Publishing, Ltd., 2011.
Original Russian Text © S.B. Dubovichenko, N. Burtebaev, D.M. Zazulin, Zh.K. Kerimkulov, A.S.A. Amar, 2011, published in Yadernaya Fizika, 2011, Vol. 74, No. 7, pp. 1013–1028.

NUCLEI
Theory

Astrophysical S Factor for the Radiative-Capture Reaction $p^6\mathrm{Li} \to {}^7\mathrm{Be}\gamma$

S. B. Dubovichenko[1)*], N. Burtebaev[2)], D. M. Zazulin[2)], Zh. K. Kerimkulov[2)], and A. S. A. Amar[3)]**

Received May 4, 2010; in final form, November 25, 2010

Abstract—A new measurement of differential cross sections for elastic p^6Li scattering in the energy range 0.35–1.2 MeV was performed. A partial-wave analysis of the data obtained in this way was carried out, and potentials simulating the p^6Li interaction were constructed. Various experiments devoted to studying elastic p^6Li scattering over the broad energy range of 0.5–50 MeV were analyzed on the basis of the optical model. By using the potentials obtained from the partial-wave analysis, the possibility of describing the astrophysical S factor for radiative proton capture on ^{6}Li at low energies was considered within the potential cluster model involving forbidden states.

DOI: 10.1134/S1063778811050073

INTRODUCTION

Experimental data on cross sections for nuclear reactions are the main source of information about the structure of nuclei and about the mechanisms of interaction between nuclei and their fragments. However, experimental investigations of such reactions at astrophysical energies are complicated by the fact that the matter-interaction energy in stars is very low, ranging between a few tenths of a keV unit and a few tens of keV units. With a few exceptions, it is next to impossible under laboratory conditions to measure directly, at such energies, nuclear-reaction cross sections, which are necessary for astrophysical calculations. Usually, cross sections are measured at higher energies, whereupon the results are extrapolated to the energy region of interest for nuclear astrophysics [1]. As a rule, however, the measurements actually performed cover only the region of rather high energies from about 0.2 to 1 MeV. In view of this, an extrapolation of such experimental data to the astrophysical region is not always justified.

As a result, only theoretical predictions can compensate in many cases for missing experimental information about the properties of astrophysical thermonuclear reactions. Under such conditions, resort to realistic models that are rather simple in practical applications, such as the potential cluster model (PCM), seems quite justified. Usually, the results of calculations performed on the basis of model concepts are contrasted against available low-energy experimental data, and approaches leading to the best agreement with these data are selected by using the results of this comparison. After that, calculations in the region of astrophysical energies are performed within the chosen conceptual framework. One can consider the results obtained in this way (for example, those concerning astrophysical S factors) as more realistic estimates of respective quantities than the extrapolation of experimental data, since the theoretical models used have, as a rule, quite a sound microscopic basis.

COMPUTATIONAL METHODS

In the present study, the results of the calculations for the astrophysical S factor for radiative proton capture on ^{6}Li are considered on the basis of the potential cluster model of light nuclei, which is constructed under the assumption that the nucleus being considered has a two-cluster structure. The choice of this model is motivated by the fact that, in many light nuclei, the probability of formation of nucleon clusters and the degree of their individualization are rather high. This is confirmed by numerous experimental data and theoretical results obtained over the past 50 years [2].

In order to calculate, on the basis of the potential cluster model, various nuclear features—for example, the astrophysical S factor for radiative proton capture on ^{6}Li at low energies—it is necessary to

[1)]Fessenkov Astrophysical Institute, National Center of Space Research and Technology, National Space Agency of the Republic of Kazakhstan, Kamenskoe plateau, Observatory 23, Almaty, 050022 Republic of Kazakhstan.
[2)]Institute of Nuclear Physics, National Nuclear Center of Republic of Kazakhstan, ul. Ibragimova 1, Almaty, 050032 Republic of Kazakhstan.
[3)]Al-Farabi Kazakh National University, pr. Al-Farabi 71, Almaty, 050038 Republic of Kazakhstan.
[*]E-mail: sergey@dubovichenko.ru
[**]E-mail: burteb@inp.kz

know intercluster-interaction potentials for the p^6Li system in various spin states. Such potentials can be constructed on the basis of elastic-scattering phase shifts, which, in turn, emerge from partial-wave analyses of experimental differential cross sections or angular distributions for the elastic scattering of the particles being considered. It is precisely the data on differential cross sections usually measured at 8 to 10 values of the scattering angle and in the required energy region that make it possible to perform the most comprehensive and precise partial-wave analysis and to obtain phase shifts for elastic scattering. Using the phase shifts obtained in the way outlined above, one can thereupon construct the required nucleus–nucleus interaction potentials, which, as is common to our calculations, must comply with the classification of orbital states according to Young tableaux [3].

The radiative-proton-capture reaction on ^{6}Li considered here is likely to be of interest for nuclear astrophysics [4]. However, the number of studies devoted to measuring the total cross section for this reaction and to experimentally determining its astrophysical S factor [5] in the region of low energies is comparatively small. Nevertheless, it is of interest to consider, on the basis of the potential cluster model and with allowance for the classification of orbital states according to Young tableaux [6], the possibility of describing the S factor for this reaction at such astrophysical energies for which there are experimental data.

In order to tackle this problem and to refine currently available experimental data, a new measurement of differential cross sections for elastic p^6Li scattering was performed in the present study for laboratory energies in the range extending up to 1.2 MeV and over a broad angular range, the errors in these measurements being 10%. On the basis of the measurements in question and the differential cross sections for elastic scattering at the energy of 500 keV from the earlier study reported in [7], we performed a partial-wave analysis and deduced the $^{2,4}S$ and ^2P phase shifts. By using the results obtained for these phase shifts, we constructed potentials for $L = 0$ and 1 in p^6Li scattering at low energies without allowance for spin–orbit splitting. After that, we performed calculations for the astrophysical S factor in the energy range between 10 keV and 1.2 MeV and compared the results of these calculations with available experimental data measured in the energy range of 35 keV–1.2 MeV.

MEASUREMENTS OF DIFFERENTIAL CROSS SECTIONS

The experimental part of the present study was performed at the UKP-2-1 electrostatic tandem accelerator of the Institute of Nuclear Physics at the National Nuclear Center of the Republic of Kazakhstan (Almaty) [8]. Protons were accelerated to laboratory energies in the range $E_p = 590$–1150 keV. The beam-current magnitude was restricted to values between 10 and 150 nA by the strength of the target used and by the admissible load of the electronics. The calibration of the proton energy in the beam was performed with the aid of reactions having narrow well-isolated resonances [9, 10]. For this purpose, we employed the reaction ^{27}Al$(p,\gamma)^{28}$Si at the energies of $E_p = 632$, 773, 992, and 1089 keV and the reaction ^{19}F$(p,\alpha\gamma)^{16}$O at the energy of $E_p = 340$ keV, the accuracy of beam calibration being ± 1 keV. The energy spread in the beam was determined by the width of the forward front of the yield curve for the reaction ^{27}Al$(p,\gamma)^{28}$Si in the vicinity of the resonance at $E_p = 992$ keV (the resonance width was smaller than 0.1 keV) and was not greater than 1.5 keV.

A beam of protons was passed through a collimating system (two collimating holes of diameter 1.5 mm at a distance of 420 mm from each other) and was focused at the target (positioned at a distance of 100 mm downstream of the last collimator) into a spot 2 mm in diameter. With the aim of minimizing the number of protons scattered off the endfaces of the collimators, the thickness of their forward walls in the region of their holes was reduced to 0.1 mm. A Faraday cylinder (a tube 15 mm in diameter and 150 mm in length) arranged at a distance of 120 mm from the target was connected to a current integrator that sent a digital pulse to a rescaling device as soon as this integrator collected a charge portion of 10 nC. The accumulated charge was determined with an error not greater than 1.5% [11, 12]. In order to minimize the formation of a carbon film on the target during the measurements, evacuation by means of magnetic-discharge and turbomolecular pumps was used along with a system of nitrogen traps arranged within the scattering chamber [13]. A typical pressure in the chamber was 1.5×10^{-6} mm Hg.

Scattered protons were recorded by a surface-barrier detector for charged particles (the diameter of the hole in the collimating diaphragm in front of the detector was 2 mm, while the thickness of the sensitive area was 0.2 mm). The detector was placed at a distance of 240 mm from the region of scattering and could be moved in the angular range from 10° to 170°. The error in determining the angle at which the detector was arranged did not exceed $\pm 0.2°$. The detector was equipped with a shielding tube that, for all of its positions, ruled out the detection of protons scattered off the endface of the last collimator and off the Faraday cylinder. The second detector, which was similar to the first one, was placed at an angle of 160° with respect to the incident-beam axis and

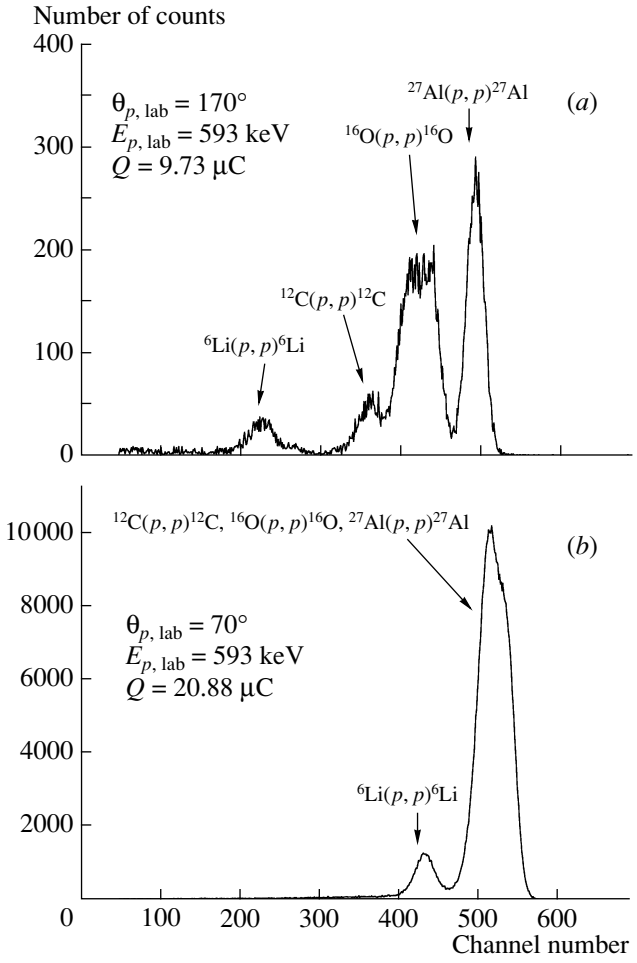

Fig. 1. Examples of spectra of protons elastically scattered on target nuclei in the process $^{6}\mathrm{Li}(p,p)^{6}\mathrm{Li}$.

was used to test the stability of the target. The energy resolution of the detectors was 15 keV.

The lithium target used in our experiment was manufactured in the following way. A layer of lithium (enriched to 96.9% in the isotope ^{6}Li) was deposited onto a backing [aluminum oxide (Al_2O_3) film obtained by the electrolytic method] by means of thermal spray-coating in a vacuum. After that, the lithium film was subjected to oxidation in the atmosphere for several minutes until stable heat-resistant compounds were formed. The thicknesses of the backing (Al_2O_3) and the lithium-oxide film were determined from a comparison of the yield curves for the reaction $^{27}\mathrm{Al}(p,\gamma)^{28}\mathrm{Si}$ in the vicinity of the resonance at $E_p = 992$ keV for two different target orientations such that the beam first traversed (i) the backing in the first case and (ii) lithium oxide in the second case. In either case, the target plane was strictly orthogonal to the incident-beam axis. After that, the thicknesses of the backing and the lithium oxide film were determined by using generally accepted values of braking parameters [14]. A target in which the thickness of the backing (Al_2O_3) was approximately identical to the thickness of the lithium oxide film (about 30 μg/cm^2) was manufactured in this way. This met the mechanical-strength and heat-resistance requirements and, at the same time, ensured a reliable separation of the $^{6}\mathrm{Li}(p,p)^{6}\mathrm{Li}$ peak from peaks due to different processes in the spectra obtained over the whole region of angles and energies covered by the experiment being discussed. For the peaks in the spectra to be separated more clearly in measurements at angles in the backward hemisphere, the target was oriented in such a way that the beam traversed first the lithium oxide film and then the backing. The target was installed at a right angle with respect to the incident-beam axis for detector positions in the angular ranges 30°–60° and 120°–170° and at an angle of 45° for detector positions in the angular range 70°–110°.

Signals from the detectors were amplified and were transferred to two 1024-channel analyzers. The dead time of the electronics did not exceed 3%. At each proton-energy value, the ratio of the area of the peak from the stationary detector because of $^{6}\mathrm{Li}(p,p)^{6}\mathrm{Li}$ scattering to the reading of the integrator counter was a constant within 5% for all positions of the movable detector. The laboratory energy was corrected with allowance for energy losses undergone by the protons traversing the lithium oxide film and the backing.

Figure 1 shows examples of spectra of protons elastically scattered off target nuclei at $E_p = 593.0$ keV. In Fig. 1*a*, one can clearly see peaks associated with elastic proton scattering on ^{6}Li, ^{12}C, ^{16}O, and ^{27}Al nuclei. The presence of a peak from the process $^{12}\mathrm{C}(p,p)^{12}\mathrm{C}$ in the spectrum in Fig. 1*a* is due to the formation of a carbon deposit on the target surface. A large width of the peak from the process $^{16}\mathrm{O}(p,p)^{16}\mathrm{O}$ in Fig. 1*a* is associated with the fact that oxygen is present both in the backing and in the lithium oxide film. Figure 1*b* shows that the peaks from the processes $^{27}\mathrm{Al}(p,p)^{27}\mathrm{Al}$, $^{16}\mathrm{O}(p,p)^{16}\mathrm{O}$, and $^{12}\mathrm{C}(p,p)^{12}\mathrm{C}$ at $E_p = 593$ keV and $\theta_p = 70°$ merge together into a single peak, but that the peak from elastic $^{6}\mathrm{Li}(p,p)^{6}\mathrm{Li}$ scattering is obviously discrete.

By the yield of elastic $^{6}\mathrm{Li}(p,p)^{6}\mathrm{Li}$ scattering, we implied the ratio of the sum of counts in the spectral peak (without preliminarily subtracted background, which we linearly approximated by a trapezoid) to the reading of the integrator counter. The statistical uncertainty in determining yields (including the uncertainty introduced by the subtracted background) was smaller than 7% for all detector positions and incident-proton energies.

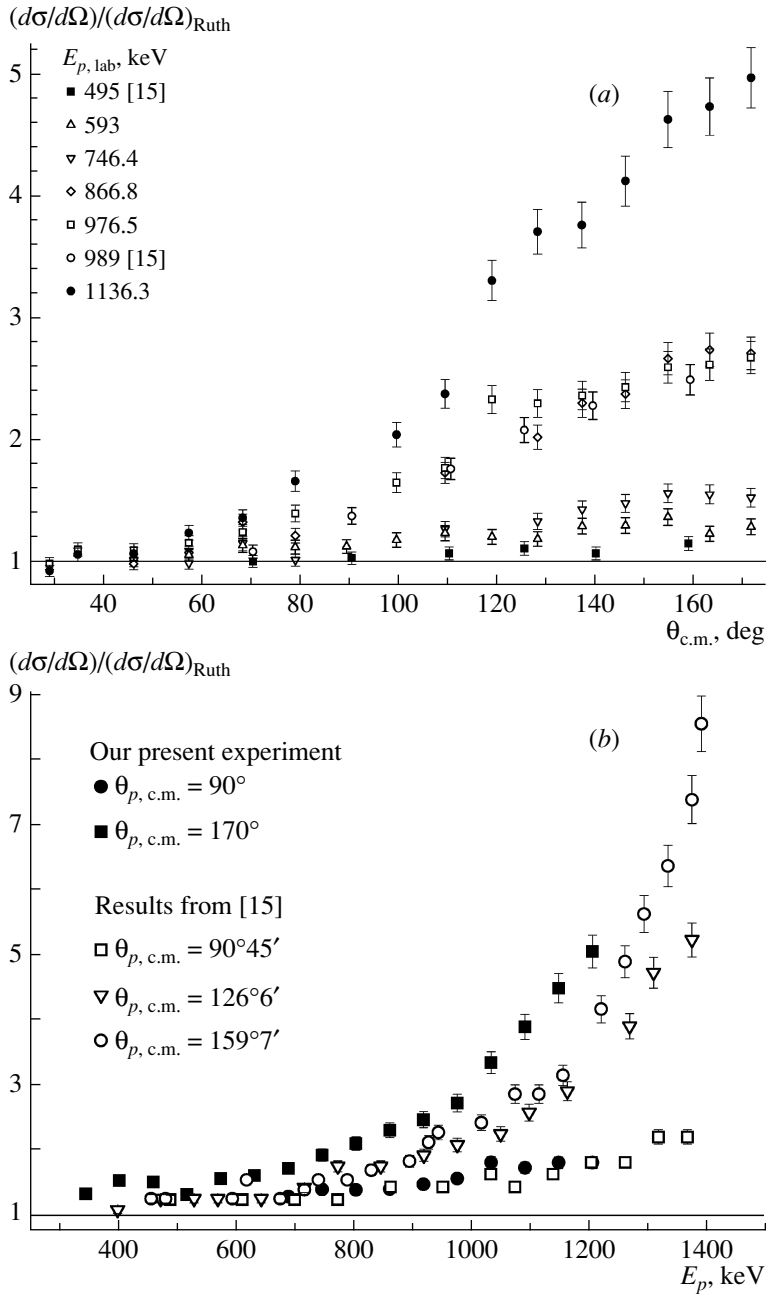

Fig. 2. (a) Differential cross sections and (b) excitation functions for the process $^6\mathrm{Li}(p,p)^6\mathrm{Li}$ according to our present study along with the results reported in [15].

In order to obtain absolute values of differential cross sections for elastic $^6\mathrm{Li}(p,p)^6\mathrm{Li}$ scattering, the yields for the angular distributions at the energies of 593.0 and 746.4 keV for angles smaller than 60° were normalized to the Rutherford cross section. To a precision of 6%, the respective normalization coefficient proved to be a constant for all energies of the present experiment. From the results of the earlier study reported in [15], it also follows that, in this region of energies and angles, the cross sections for the elastic-scattering process $^6\mathrm{Li}(p,p)^6\mathrm{Li}$ differ from the Rutherford cross sections by not more than 5%. The systematics given below for the parameters of the optical potential for elastic $p^6\mathrm{Li}$ scattering confirms the reliability of our experimental data.

The differential cross sections obtained in the present study and divided by the Rutherford cross sections are displayed in Fig. 2a along with data from [15]. The absolute values of the excitation functions were calculated by using the normalization

coefficient obtained here. The ratios of the excitation functions to the Rutherford cross sections are presented in Fig. 2*b* along with data from [15]. The total uncertainty in the experimental data presented in Fig. 2 did not exceed 10%.

Thus, the differential cross sections for the elastic-scattering process ^{6}Li$(p,p)^6$Li (angular distributions) were measured at the following five energy values: 593.0 keV at 12 angles in the range 60°–170°, 746.4 and 866.8 keV at 11 angles in the range 45°–170°, and 976.5 and 1136.3 keV at 15 angles in the range 30°–170°. The excitation functions for ^{6}Li$(p,p)^6$Li were measured in the energy range $E_p = 345$–1206 keV with a step of 50 keV for two angles of 90° and 170° in the c.m. frame.

OPTICAL MODEL

The data obtained in the present study were analyzed on the basis of the standard optical model of the nucleus [16] along with some other data on elastic p^6Li scattering at energies from 0.5 to 50 MeV. In this model, the effect of inelastic channels is taken into account phenomenologically by introducing an absorptive imaginary part in the interaction potential that describes colliding nuclei, while elastic scattering is described by a complex interaction potential whose radial dependence is taken in the Woods–Saxon form

$$U(r) = -V_0 f(x_V) - i[W f(x_W)] + V_C(r),$$

where

$$f(x_i) = (1+\exp(x_i))^{-1},$$
$$x_i = (r - R_i)/a_i, \quad R_i = r_i A^{1/3};$$

the subscript i assumes the value of V (distribution for the real part of the potential) and the values of W (distribution for the imaginary part of the potential); and $V_C(r)$ is the Coulomb potential of a uniformly charged sphere of radius $R = 1.28A^{1/3}$ [fm] [16]. The parameters of the optical potential (OP) were chosen in such a way as to attain the best agreement between the calculated and experimental angular distributions. Automatic searches for optimum optical-potential parameters were performed by minimizing the parameter χ^2/N with the aid of the SPI-GENOA code [17].

In order to choose optimum optical-potential parameters, we constructed a systematics of the experimental data obtained in the present study and in [18–20] on elastic p^6Li scattering in the energy range of $E_p = 0.5$–50 MeV. A global systematics for the potential simulating proton interaction with nuclei was presented earlier in [21]. This systematics works well in the case of medium-mass and heavy nuclei; in the case of extremely light nuclei—for example, nuclei of lithium isotopes—it is necessary to take into account a strong deviation of the geometric parameters of the potential from their averaged values obtained from the global systematics. Since the optical-potential parameters to be established were intended for use at low energies and since, in this energy region, proton–nucleus interaction occurs mainly in the superficial region, an optical potential involving a surface-type absorption W_D [16] was employed in the calculations of scattering cross sections. A spin–orbit component was included in the complex potential because both an incident particle and a target nucleus have spins.

A preliminary analysis of data on elastic scattering on the basis of the optical model over a broad energy range showed that the use of the following radii for the real and imaginary parts of the potential is the most correct:

$$r_0 = 1.05 \text{ fm}, \quad r_D = 1.923 \text{ fm}.$$

In the following, the choice of remaining optical-potential parameters is performed with the radii fixed at these values. The energy dependence of the real (V_0) and imaginary (W_D) parts of the potential is studied at the center of the nucleus.

The following linear dependences of the optical-potential parameters V_0 and W_D were obtained for the p^6Li system [16]:

$$V_0 = 56.10 \text{ MeV} - 0.61E_p \text{ (MeV)},$$
$$W_D = -0.66 \text{ MeV} + 0.46E_p \text{ (MeV)}.$$

A discrete ambiguity in the potential parameter V_0 at low energies was removed by using the energy dependence of the depth of the real part of the potential and by comparing V_0 with its value extracted from the calculations of the volume integral J_R of the optical potential according to data on nucleon–nucleon scattering [22].

Since both a scattered particle and a target nucleus have a spin, we also take into account the contribution of spin–orbit interaction (V_S, r_S, and a_S are, respectively, the depth, radius, and diffuseness parameter of the spin–orbit potential) in calculating differential cross sections for the scattering process being considered. The results calculated within this approach for the parameters of the optical potential simulating the interaction are presented in Table 1. Some calculated cross sections for elastic proton scattering on ^{6}Li nuclei are given in Fig. 3. This figure shows that agreement between the theoretical and experimental results is good over the whole angular range and over a broad energy range.

Table 1. Optimum parameters of the optical potential for elastic p^6Li scattering

E_p, MeV	V_0, MeV	a_0, fm	W_D, MeV	a_D, fm	V_S, MeV	r_S, fm	a_S, fm	J_R, MeV fm^3	J_W, MeV fm^3
0.500	59.0	0.85	0.30	0.575	9.3	1.077	0.66	623	19.22
0.7464	57.2	0.67	0.355	0.65	9.3	1.02	0.20	616	26.0
0.9765	56.3	0.68	0.355	0.57	9.3	1.02	0.20	454	22.19
3	55.08	0.78	0.87	0.575	9.3	1.02	0.20	437	55.72
5	52.0	0.93	1.18	0.82	15.6	1.02	0.77	407	75.58
10	50.0	0.90	2.78	0.654	4.66	1.02	0.20	391	148.3
12	47.52	0.550	5.03	0.49	12.23	1.02	0.20	415	282
14	46.86	0.85	6.72	0.423	9.86	1.02	0.20	378	304
25	38.99	0.65	3.89	0.547	5.517	1.02	0.20	270	309
29.9	37.16	0.75	2.5	0.654	2.816	1.02	0.20	149	111
35	33.35	0.67	2.9	0.66	3.65	1.02	0.20	142	111
45	30.0	0.71	2.96	0.69	2.33	1.02	0.20	122	100
49.9	24.55	0.87	1.58	0.516	2.13	1.02	0.266	64	106

Note: Here, J_W is the volume integral of the imaginary part of the optical potential.

DIFFERENTIAL CROSS SECTIONS AND PHASE SHIFTS

In order to perform a partial-wave analysis of elastic scattering in the system of particles whose spins are $1/2 + 1$—for example, in the p^2H or p^6Li system—without taking into account the spin–orbit splitting of phase shifts, the scattering cross section can be written in a rather simple form [16],

$$\frac{d\sigma(\theta)}{d\Omega} = \frac{2}{6}\frac{d\sigma_d(\theta)}{d\Omega} + \frac{4}{6}\frac{d\sigma_k(\theta)}{d\Omega}, \qquad (1)$$

where the indices d and k refer to, respectively, the doublet ($S = 1/2$) and quartet ($S = 3/2$) states of the p^6Li system. Each of these differential cross sections can be expressed in terms of the respective scattering amplitudes as

$$\frac{d\sigma_d(\theta)}{d\Omega} = |f_d(\theta)|^2, \quad \frac{d\sigma_k(\theta)}{d\Omega} = |f_k(\theta)|^2. \qquad (2)$$

The amplitudes in question have the form [16]

$$f_{d,k}(\theta) = f_{\rm C}(\theta) + f^N_{d,k}(\theta), \qquad (3)$$

where

$$f_{\rm C}(\theta) = -\left(\frac{\eta}{2k\sin^2(\theta/2)}\right) \qquad (4)$$
$$\times \exp\{i\eta\ln[\sin^{-2}(\theta/2)] + 2i\sigma_0\},$$
$$f^N_d(\theta) = \frac{1}{2ik}\sum_L (2L+1)$$
$$\times \exp(2i\sigma_L)[S^d_L - 1]P_L(\cos\theta),$$
$$f^N_k(\theta) = \frac{1}{2ik}\sum_L (2L+1)$$
$$\times \exp(2i\sigma_L)[S^k_L - 1]P_L(\cos\theta),$$

and $S^{d,k}_L = \eta^{d,k}_L \exp[2i\delta^{d,k}_L(k)]$ is the scattering matrix in the spin-doublet or spin-quartet state [16].

The possibility of employing, in our analysis, the simple expressions (1)–(4) to calculate elastic-scattering cross sections is due to the fact that, in the low-energy region extending up to 1.0 or 1.2 MeV, the spin–orbit splitting of phase shifts is relatively small, this being confirmed by the results of the earlier partial-wave analysis performed in [23] with allowance for spin–orbit splitting at energies of up to 2.5 MeV.

Knowing experimental values of the differential cross sections for elastic scattering, we can always find a set of parameters (phase shifts $\delta^J_{S,L}$) that makes it possible to describe the behavior of these cross sections to some degree of precision. The quality of the description of experimental data on the basis of some theoretical function (functional of several variables) can be estimated by the χ^2 method. The functional χ^2 can be represented in the form [16]

$$\chi^2 = \frac{1}{N}\sum_{i=1}^{N}\left[\frac{\sigma^t_i(\theta) - \sigma^e_i(\theta)}{\Delta\sigma^e_i(\theta)}\right]^2 = \frac{1}{N}\sum_{i=1}^{N}\chi^2_i,$$

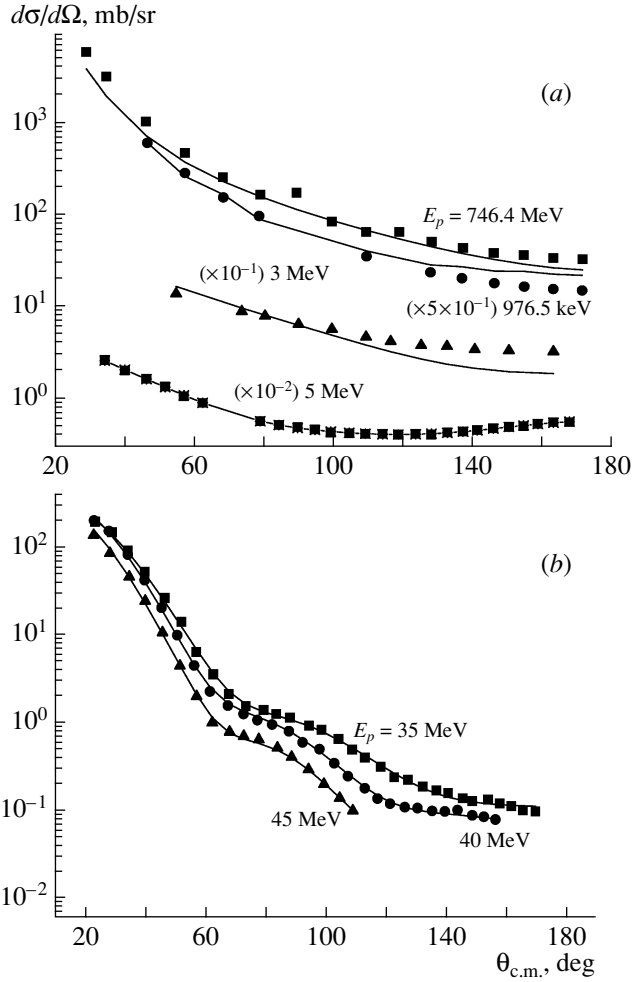

Fig. 3. Differential cross sections for elastic protons scattering on ^{6}Li nuclei at various values of E_p. The displayed points stand for experimental data obtained in the present study and those borrowed from [18–21]. The curves represent the results of the calculations based on the optical model (see main body of the text).

where σ^e and σ^t are, respectively, the experimental and the theoretical (that is, calculated at some preset values of the phase shifts $\delta^J_{S,L}$) cross section for the elastic scattering of nuclear particles at the ith scattering angle, $\Delta\sigma^e$ is the error in the experimental cross sections at this angle, and N is the number of measurements.

As a matter of fact, the expressions that describe differential cross sections are an expansion of a functional $d\sigma(\theta)/d\Omega$ in a numerical series, and it is necessary to find such variational parameters δ of the expansion that ensure the best description of the experimental data, in just the same way as this was done in [24].

In all calculations, we used precise values of particle masses [25] and set the constant $\hbar^2/m_0$ to 41.4686 MeV fm^2. The Coulomb parameter $\eta = \mu Z_1 Z_2 e^2/(q\hbar^2)$ was represented in the form $\eta = 3.444\,76 \times 10^{-2} Z_1 Z_2 \mu/q$, where q is the wave number (in fm^{-1} units) determined by the energy of interacting particles in the entrance channel. The Coulomb potential at $R_C = 0$ was written in the form $V_C(\mathrm{MeV}) = 1.439\,975 Z_1 Z_2/r$, where r is the distance between the particles in the entrance channel (in fm units). The numerical and variational methods that were used to obtain the present results were described in detail elsewhere [26].

PARTIAL-WAVE ANALYSIS

A partial-wave analysis of the excitation functions for elastic p^6Li scattering at low energies was performed in [23] with allowance for spin–orbit splitting but without taking explicitly into account the doublet ^2P wave. Our partial-wave analysis is based on data on differential cross sections from the present study and from the earlier study reported in [7] and is performed at energies below 1.2 MeV, which are

Table 2. Results of our partial-wave analysis for elastic p^6Li scattering at astrophysical energies

No.	E_p, keV (lab. frame)	^2S, deg	^4S, deg	^2P, deg	^4P, deg	χ^2
1	500	176.2	178.7	–	–	0.15
2	593	174.2	178.8	–	–	0.15
3	746.4	170.1	180.0	–	–	0.23
	746.4	172.5	179.9	1.7	0.0	0.16
4	866.8	157.8	180.0	–	–	0.39
	866.8	170.2	174.9	3.9	0.0	0.22
	866.8	169.6	175.0	3.5	<0.1	0.23
5	976.5	160.0	178.5	–	–	0.12
	976.5	167.0	174.5	1.1	0.0	0.12
6	1136.3	144.9	180.0	–	–	0.58
	1136.3	164.7	171.1	5.8	0.0	0.32
	1136.3	166.4	169.9	5.5	∼0.1	0.32

of importance for nuclear astrophysics. This analysis takes into account all of the lowest partial waves, including the doublet ^2P wave.

At the energy of 500 keV, we found ^2S and ^4S phase shifts (see Table 2) on the basis of data from [7], the χ^2 value averaged over all measurements being $\chi^2 = 0.15$. In order to determine χ^2, the error in the differential cross sections was taken to be 10% for these data. An attempt at taking into account the doublet ^2P- and quartet ^4P-wave phase shifts revealed that their numerical values are smaller than 0.1°.

The following five energies correspond to the results obtained in the present study by measuring the differential cross sections for elastic scattering. For the first of them, 593 keV, we found $^{2,4}S$ phase shifts differing only slightly from their counterparts at the preceding energy value and having the same value of χ^2 (see Table 2); we also found that the $^{2,4}P$-wave phase shifts are negligible.

At the energy of 746.4 keV, we found the $^{2,4}S$-wave phase shifts (Table 2), which enabled us to describe the cross sections with $\chi^2 = 0.23$. Despite the smallness of the parameter χ^2, we made an attempt at taking into account the $^{2,4}P$ wave. Previously, it was assumed that the quartet ^4P-wave phase shift is zero, as follows from the results reported in [23], where the ^4P wave was taken into account starting from 1.0 or 1.5 MeV. The results of our analysis performed with allowance for only the ^2P-wave phase shift are given in Fig. 4*a* and in Table 2. One can readily see that the inclusion of a moderately small doublet ^2P wave changes somewhat the doublet ^2S-wave phase shift, increasing its value and decreasing the parameter χ^2, which becomes 0.16. Further, the inclusion of the quartet ^4P-wave phase shift led to a negligible value below 0.1°.

The results of our searches for phase shifts at the energy of 866.8 keV with allowance for only the $^{2,4}S$ waves ($^{2,4}P = 0$) are given in Table 2, the respective χ^2 value being $\chi^2 = 0.39$. One can readily see that the ^2S-wave phase shift is much smaller than that at the preceding energy value. But the inclusion of the ^2P wave increases its value sizably (see Fig. 4*b* and Table 2) and decreases the parameter χ^2 nearly by a factor of two. An attempt at taking into account the quartet ^4P-wave phase shift led to its value not greater than 0.1° (see Table 2). Any variation in the ^4P phase shift toward greater values led to an increase in the parameter χ^2 even in the case of different values of the remaining phase shifts. At this energy, as well as in the case of the other energies considered here, we did not find any version of the set of phase shifts where the quartet phase shift is nonzero. It always goes to zero as the parameter χ^2 approaches its minimum value.

For the next energy value of 976.5 keV, our analysis performed without allowance for the $^{2,4}P$ waves yielded the $^{2,4}S$-wave phase shifts listed in Table 2. The subsequent inclusion of the ^2P wave also increases considerably the values of the ^2S-wave phase shifts (see Fig. 4*c* and Table 2), the respective χ^2 value being $\chi^2 = 0.12$.

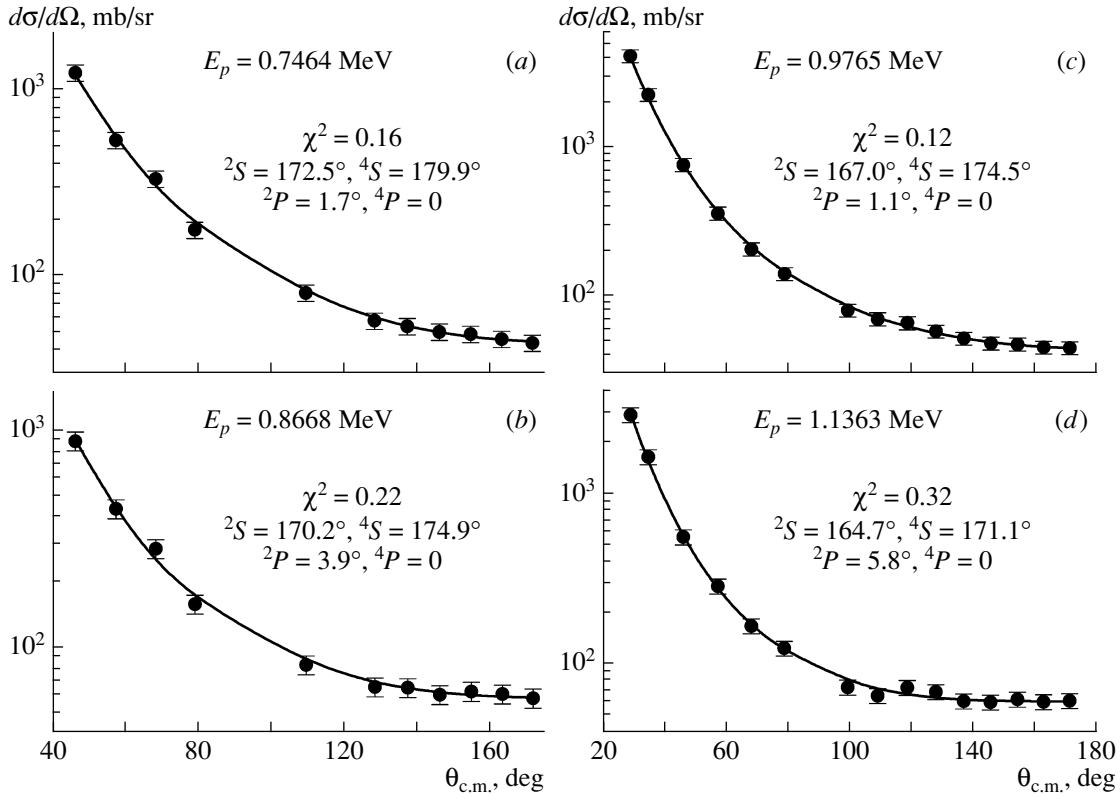

Fig. 4. Cross sections for elastic p^6Li scattering at the energies of (*a*) 746.4, (*b*) 866.8, (*c*) 976.5, and (*d*) 1136.3 keV. The displayed points stand for experimental data obtained in our present study. The curves represent cross sections calculated by using values found here for phase shifts (see main body of the text).

The last energy value considered here, 1.1363 MeV, leads to a comparatively small value of χ^2 (0.58) even if we take into account only $^{2,4}S$ waves (see Table 2). However, the inclusion of the ^2P wave decreases this value sizably. The results of the calculations for cross sections are presented in Fig. 4*d* and in Table 2. In this case, the inclusion of ^2P wave also leads to a sizable increase in the value of the ^2S-wave phase shift, while the inclusion of the ^4P-wave phase shift leads to small values of this quantity.

Thus, we see that, in the energy region being considered, the quartet ^4P waves are not necessary for describing the entire body of experimental data obtained here (the corresponding phase shifts are equal to or smaller than 0.1°). By and large, this agrees with the results reported in [23], but the doublet ^2P-wave phase shift almost reaches a value of 6°, with the result that its explicit inclusion affects significantly the intensity of the doublet ^2S wave. A general pattern of the ^2S and ^4S-wave phase shifts is shown in Fig. 5*a*, while the doublet ^2P-wave phase shifts are given in Fig. 5*b*. In spite of a rather large scatter of the results for the ^4S-wave phase shifts, the doublet ^2S-wave phase shift shows a trend toward a decrease, but the rate of this decrease is considerably lower than what one could expect from the results of the analysis in [23]. If we do not take into account the doublet ^2P wave in our analysis, the results for the ^2S-wave phase shifts appear to be very close to the results of the partial-wave analysis performed in [23].

The errors in the phase shifts for elastic scattering are determined by the presence of an ambiguity in the results of our partial-wave analysis—namely, somewhat different values of the phase shifts can be obtained at χ^2 values differing by not more than 5 to 10%. We estimate this ambiguity at 1° to 1.5° and illustrate it for the $^{2,4}S$- and ^2P-wave phase shifts in Figs. 5*a* and 5*b*.

CLASSIFICATION OF CLUSTER STATES

Let us consider the Young tableau classification of orbital and spin or isospin states of the p^6Li cluster system bound in the ^{7}Be nucleus. In general, the possible orbital Young tableau $\{f\}$ for a certain nucleus $A(\{f\})$ consisting of two components, $A_1(\{f_1\}) + A_2(\{f_2\})$, is given by the direct outer product of the orbital Young tableaux for these components, $\{f\}_L = \{f_1\}_L \times \{f_2\}_L$, and is determined according to the

Littlewood theorem [27]. The spin–isospin tableaux for a nucleus are the direct inner product of its spin S and isospin T Young tableaux, $\{f\}_{ST} = \{f\}_S \otimes \{f\}_T$ [27, 28]. For the p^6Li channel of the ^{7}Be nucleus, the respective tableaux are presented in Table 3, while, for an arbitrary system containing two to eight particles, they are given in [28]. For any of these moments (S or T), the corresponding tableau for a nucleus including A nucleons, each having a moment equal to 1/2, is constructed according to the rules known from [29]. By way of example, we indicate that, for the ground state of the ^{7}Be nucleus, whose moment is 3/2, we have the tableau {52}, while, for a specific state of moment 1/2, we have the tableau {43}.

The complete Young tableau for a nucleus is defined in just the same way as in the case of spin–isospin symmetry—that is, as the direct inner product of the orbital and spin–isospin components: $\{f\} = \{f\}_L \otimes \{f\}_{ST}$. Under antisymmetrization, the respective wave function is not identically zero only if it contains an antisymmetric component $\{1^A\}$, which is the case if one multiplies conjugate tableaux $\{f\}_L$ and $\{f\}_{ST}$. Therefore, the orbital tableaux $\{f\}_L$ conjugate to $\{f\}_{ST}$ are assumed to be allowed in this channel, while all of the remaining orbital symmetries are forbidden because they lead to a zero total wave function for the system of particles upon its antisymmetrization.

If the tableau {6}, which is forbidden in the ^{2}H^{4}He channel, is used for the ^{6}Li nucleus, the possible orbital Young tableaux for the p^6Li system also appear to be forbidden. They correspond to forbidden states having configurations {7} and {61} and orbital angular momenta of relative motion that are determined according to the Elliott rule [27] ($L = 0$ and 1). These symmetries are forbidden for the wave function by the general requirement of the Littlewood theorem that not more than four cells be present in a row of the corresponding tableaux [27].

If, for the ^{6}Li nucleus, we take the tableau {42} allowed in the ^{2}H^{4}He cluster channel, then, for the total system p^6Li of spin $S = 1/2$, there are a forbidden level corresponding to the tableau {52} and having orbital angular momenta of $L = 0$ and 2 and allowed states corresponding to the configurations {43} and {421} and having the orbital angular momentum of $L = 1$. Thus, p^6Li potentials must involve the {52} forbidden bound state in the S wave and the allowed bound level appearing in the P wave and corresponding to two Young tableaux, {43} and {421}. In the quartet spin state of this system, only one tableaux, {421}, is allowed, as is shown in Table 3.

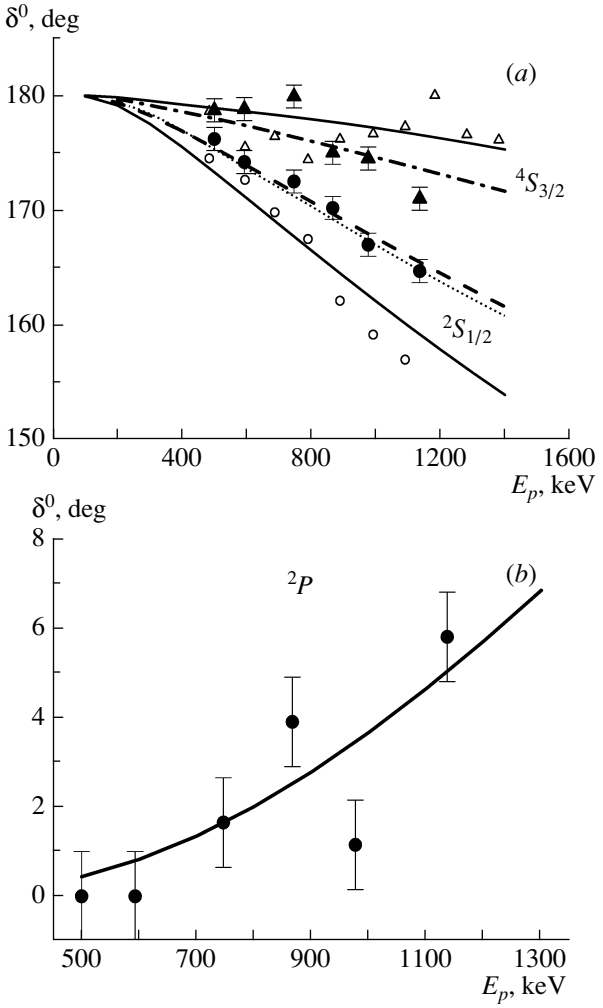

Fig. 5. (a) Doublet and quartet $^{2,4}S$-wave phase shifts for elastic p^6Li scattering at low energies in the presence of the ^2P wave for the case where the ^4P-wave phase shift is taken to be zero: (closed circles and triangles) results of our present analysis for, respectively, the ^2S- and ^4S-wave phase shifts; (open circles triangles) results of the partial-wave analysis performed in [23]; (curves) results of the calculations with various potentials (see main body of the text). (b) Doublet ^2P-wave phase shifts for elastic p^6Li scattering at low energies: (points) results of our present partial-wave analysis for the ^2P-wave phase shifts at $^4P = 0$ and (curve) result of the calculations with the potential found in our study (see main body of the text).

Possibly, it is more correct to consider, for the bound states of the ^{6}Li nucleus, both of the allowed tableaux {6} and {42} because both are present in the forbidden and allowed states of this nucleus in the ^{2}H^{4}He configuration [30]. This leads to a somewhat different classification of levels: the number of forbidden states increases, an extra forbidden bound level appearing in each partial wave. This, wider, scheme of levels is given in Table 3. As a matter of fact, it is a

Table 3. Classification of orbital states in the p^6Li and n^6Li systems

System	T	S	$\{f\}_T$	$\{f\}_S$	$\{f\}_{ST} = \{f\}_S \otimes \{f\}_T$	$\{f\}_L$	L	$\{f\}_{\rm AS}$	$\{f\}_{\rm FS}$
n^6Li	1/2	1/2	{43}	{43}	{7} + {61} + {52}	{7}	0	–	{7}
p^6Li					+ {511} + {43}	{61}	1	–	{61}
					+ {421} + {4111}	{52}	0, 2	–	{52}
					+ {322} + ***{3211}***	***{43}***	1, 3	{43}	–
					+ ***{2221}*** + {331}	***{421}***	1, 2	{421}	–
		3/2	{43}	{52}	{61} + {52} + {511}	{7}	0	–	{7}
					+ {43} + 2{421}	{61}	1	–	{61}
					+ {331} + {322}	{52}	0, 2	–	{52}
					+ ***{3211}***	{43}	1, 3	–	{43}
						{421}	1, 2	{421}	–

Note: Here, T, S, and L are, respectively, the isospin, spin, and orbital angular momentum of the p+^{6}Li two-particle system; $\{f\}_S$, $\{f\}_T$, $\{f\}_{ST}$, and $\{f\}_L$ are, respectively, the spin, isospin, spin–isospin [28], and possible orbital Young tableaux; and $\{f\}_{\rm AS}$ and $\{f\}_{\rm FS}$ are the Young tableaux for, respectively, the allowed and forbidden orbital states. The Young tableaux $\{f\}_{ST}$ and $\{f\}_L$ conjugate to each other are printed in boldface italics.

sum of the first and the second of the above cases. The total spin ($\{f\}_S$) and isospin ($\{f\}_T$) Young tableaux for the ^{7}Be nucleus in the p^6Li channel are shown in Table 3 along with their product $\{f\}_{ST}$ and all possible orbital symmetries $\{f\}_L$ of the p^6Li system, which are broken down into allowed ($\{f\}_{\rm AS}$) and forbidden ($\{f\}_{\rm FS}$) tableaux, the respective values of the orbital angular momentum L being indicated.

From the data in Table 3, it follows that, in the doublet spin state of the p^6Li system, there are two allowed tableaux {43} and {421}, so that scattering states appear to be mixed in orbital symmetries. At the same time, it is common practice to believe [2, 6, 31] that only one allowed tableau {43} corresponds to the doublet ground state of the ^{7}Be nucleus in the p^6Li channel for $J = 3/2^-$ and $L = 1$. There is a perfect analogy between the system in question and the p^2H channel in the ^{3}He nucleus [6, 31], whose doublet state is mixed in the Young tableaux {3} and {21}. Therefore, the potentials that are constructed on the basis of fits to the phase shifts for elastic scattering in the p^6Li system cannot be used to describe the properties of the ground state of the ^{7}Be nucleus.

In just the same way as in the case of the p^2H system, the phase shifts for elastic p^6Li scattering are then represented as the half-sum of the pure phase shifts [2, 32]; that is,

$$\delta_L^{\{43\}+\{421\}} = 1/2\delta_L^{\{43\}} + 1/2\delta_L^{\{421\}}.$$

The mixed phase shifts are determined from a partial-wave analysis of experimental data, which are usually differential cross sections for elastic scattering or excitation functions. Further, it is assumed [6, 31] that the phase shifts of the same symmetry from the quartet channel can be used for the {421} pure phase shifts of the doublet channel. As a result, one can find the {43} pure doublet phase shifts for p^6Li scattering and, on this basis, construct an interaction corresponding to the potential for the bound state of the p^6Li system in the ^{7}Be nucleus [32].

DESCRIPTION OF PHASE SHIFTS IN TERMS OF POTENTIALS

In order to construct partial intercluster p^6Li interactions on the basis of available phase shifts, we use an ordinary Gaussian potential supplemented with a pointlike Coulomb term; that is,

$$V(R) = -V_0 \exp(-\alpha R^2).$$

From a fit to the results of the partial-wave analysis performed in [23], we obtained the parameter values

$$V_0 = 110 \text{ MeV and } \alpha = 0.15 \text{ fm}^{-2}$$

for the ^2S-wave phase shift and

$$V_0 = 190 \text{ MeV and } \alpha = 0.2 \text{ fm}^{-2}$$

for the ^4S-wave phase shift.

Each potential involves two forbidden bound states corresponding to the Young tableaux {52} and {7} [3, 32]. The phase shifts calculated with these potentials are shown in Fig. 5*a* by solid curves along with the

results of the partial-wave analysis performed in [23] (open circles and triangles).

In order to describe the scattering phase shifts obtained in our partial-wave analysis, it is preferable to use the potentials whose parameter take the values

$$V_0 = 126 \text{ MeV and } \alpha = 0.15 \text{ fm}^{-2}$$
$$\text{for the } {}^2S\text{-wave phase shift}$$
$$\text{and } V_0 = 142 \text{ MeV and } \alpha = 0.15 \text{ fm}^{-2}$$
$$\text{for the } {}^4S\text{-wave phase shift.}$$

These potentials also include two forbidden bound states each, the respective orbital Young tableaux being {52} and {7}. The phase shifts calculated by using the potentials in question are shown in Fig. 5*a* by the dashed and dash-dotted curves along with the results of our partial wave analysis (closed circles and triangles). The potential for doublet ${}^2P$-wave scattering can be characterized, for example, by the parameter values

$$V_0 = 68.0 \text{ MeV}, \quad \alpha = 0.1 \text{ fm}^{-2}.$$

In Fig. 5*b*, the phase shifts calculated on the basis of this potential, which involves one forbidden bound state corresponding to the Young tableau {61} and one allowed state corresponding to two Young tableaux {43} and {421}, are represented by the solid curve. This potential leads to incorrect values for the binding energy of the ^{7}Be nucleus in the p^6Li channel because the allowed state appears to be mixed in the above two symmetries, while only one tableau {43} corresponds to the ground bound state of the ^{7}Be nucleus [3]. But even if use is made of the aforementioned methods for deducing pure phase shifts, a ground-state potential pure in Young tableaux could not be determined.

In view of this, a ${}^2P_{3/2}$-wave potential pure in the orbital symmetry {43} for the ground state of the ^{7}Be nucleus in the p^6Li channel was constructed in such a way as to describe, first of all, the channel energy—that is, the binding energy of the $J = 3/2^-$ ground state of the ^{7}Be nucleus as the p^6Li system—and its root-mean-square charge radius. The values obtained in this way for the parameters of the pure doublet ${}^2P_{3/2}^{\{43\}}$ potential are

$$V_P = 252.914\,744 \text{ MeV}, \quad \alpha_P = 0.25 \text{ fm}^{-2}. \quad (5)$$

The potential, used together with the finite-difference method [26], yields a value of 5.605 800 MeV for the binding energy of the allowed state (the corresponding experimental value is 5.605 8 MeV [33]) and involves one forbidden state corresponding to the Young tableau {61}. The root-mean-square charge radius is 2.63 fm, which agrees, on the whole, with data reported in [33]. The asymptotic constant C_W determined on the basis of Whittaker functions,

$$\chi_L(R) = \sqrt{2k_0} C_W W_{-\eta L+1/2}(2k_0 R),$$

in the interval 5–13 fm is 2.66(1). The error given here for the asymptotic constant was determined via averaging its values over the above interval of distances. Here, $\chi_L(R)$ is the numerical bound-state wave function obtained by solving the radial Schrödinger equation and normalized to unity; $W_{-\eta L+1/2}$ is the Whittaker function characterizing the bound state, determining the asymptotic behavior of this wave function, and appearing to be a solution of the same equation but without the nuclear potential—that is, at large distances; k_0 is the wave number determined by the channel binding energy; η is the Coulomb parameter; and L is the orbital angular momentum of the bound state.

For the parameters of the ${}^2P_{1/2}^{\{43\}}$ potential for the $J = 1/2^-$ first excited state of the ^{7}Be nucleus in the p^6Li channel, we obtained the values

$$V_P = 251.029\,127 \text{ MeV}, \quad \alpha_P = 0.25 \text{ fm}^{-2}. \quad (6)$$

This potential leads to the binding-energy value of 5.176 700 MeV (the respective experimental value is 5.176 7 MeV [33]) and involves a forbidden state associated with the tableaux {61}. The asymptotic constant in the interval 5–13 fm is 2.53(1), and the root-mean-square charge radius is 2.64 fm.

In the calculations by the finite-difference method, the absolute accuracy in searches for the energies of bound-state levels of the p^6Li system in the ^{7}Be nucleus was preset at a level of 10^{-6} MeV. The values obtained here for the parameters of the bound-state potentials differ somewhat from the previous results reported in [3]. This is due to employing precise particle-mass values in the present calculations and obtaining a more accurate description of experimental energies of levels.

In order to test additionally the accuracy in calculating the binding energy, we used the variational method, expanding the radial wave function for the p^6Li system in a nonorthogonal Gaussian basis and varying the parameters involved independently [32, 34]. For the basis dimension of $N = 10$, we obtained the value of $-5.605\,797$ MeV for the ground-state energy. Since, in response to an increase in the basis dimension, variational energy decreases, yielding an upper limit on the true binding energy, and since the energy from finite-difference calculations increases as the step decreases while the number of steps increases [26], we can take the average value of $-5.605\,798\,5(15)$ MeV for the actual binding energy

in this potential. Thus, the actual accuracy in calculating the binding energy in the preset potential is ± 1.5 eV for both methods. The asymptotic constant appears to be relatively stable in the interval 5–13 fm, amounting to 2.67(2), while the value of the charge radius agrees with the result of the finite-difference calculations.

For the ground state of the ^{7}Be nucleus in the p^6Li channel with the Gaussian potential (5), the parameters of the radial variational wave function describing the relative motion of the clusters and having the form [31]

$$\Phi_L(R) = \frac{\chi_L(R)}{R} = R^L \sum_i C_i \exp(-\beta_i R^2)$$

are given in Table 4, the residual not exceeding 10^{-12} [26].

The value obtained by the variational method for the energy of the first excited level is $-5.176\,697$ MeV, so that the average energy is $-5.176\,698\,5(15)$ MeV, the corresponding precision being identical to that in the case of the ground state for both methods. The asymptotic constant in the interval 5–13 fm is at the level of 2.53(2), the residual not exceeding 10^{-12}, while the charge radius does not differ from the corresponding value obtained by the finite-difference method. The parameters of the wave function for the first excited state of the ^{7}Be nucleus in the p^6Li channel for the potential in (6) are presented in Table 5.

ASTROPHYSICAL S FACTOR

The astrophysical S factor was analyzed with allowance for the $E1$ transitions from the ^2S- and ^2D-wave states of p^6Li scattering to the $^2P_{3/2}$ ground and the $^2P_{1/2}$ first excited bound state of the ^{7}Be nucleus in the p^6Li channel. The calculation of the wave function for the ^2D scattering state without allowance for spin–orbit splitting was performed on the basis of the ^2S-wave potential at $L = 2$.

In order to calculate the astrophysical S factor, we employed the standard expression [35]

$$S(NJ, J_f) = \sigma(NJ, J_f) E_{\rm cm} \times \exp\left(\frac{31.335 Z_1 Z_2 \sqrt{\mu}}{\sqrt{E_{\rm cm}}}\right),$$

which was proposed as far back as the 1950s in [36] and where σ is the total cross section for the radiative-capture process (in barn units), $E_{\rm cm}$ is the c.m. energy of particles in the entrance channel (in keV units), μ is the reduced mass of the entrance-channel particles (in atomic mass units), Z are the charges of the particles (in elementary charge units, e) and N stands for E (electric) or M (magnetic) transitions of multipolarity J to the final (J_f) state of the nucleus. The numerical coefficient 31.335 was obtained by the present authors on the basis of modern values of fundamental constants from [37].

In the above expression for the S factor, we isolated explicitly quickly changing exponential factor $P(E)$ generated by the Coulomb barrier. In response to the change in the energy, the S factor therefore changes much more slowly than the cross sections. The factorization of the cross section in the form

$$\sigma(NJ, J_f) = S(NJ, J_f) P(E)$$

simplifies considerably the behavior of the S factor as a function of energy [1] even in the resonance region.

In the potential cluster model, the total radiative-capture cross sections $\sigma(NJ, J_f)$ have the form (see, for example, [5] or [31])

$$\sigma_c(NJ, J_f) = \frac{8\pi K e^2}{\hbar^2 q^3} \frac{\mu}{(2S_1+1)(2S_2+1)} \times \frac{J+1}{J[(2J+1)!!]^2} A_J^2(NJ, K) \times \sum_{L_i, J_i} P_J^2(NJ, J_f, J_i) I_J^2(J_f, J_i),$$

where, for electric orbital [$EJ(L)$] transitions ($S_i = S_f = S$), we have

$$P_J^2(EJ, J_f, J_i) = \delta_{S_i S_f} [(2J+1)(2L_i+1)(2J_i+1)(2J_f+1)] \times (L_i 0 J 0 | L_f 0)^2 \begin{Bmatrix} L_i & S & J_i \\ J_f & J & L_f \end{Bmatrix}^2,$$

$$A_J(EJ, K) = K^J \mu^J \left(\frac{Z_1}{m_1^J} + (-1)^J \frac{Z_2}{m_2^J}\right),$$

$$I_J(J_f, J_i) = \langle \chi_f | R^J | \chi_i \rangle .$$

Here, q is the wave number of entrance-channel particles; L_f, L_i, J_f, and J_i are the particle angular momenta in the entrance (i) and exit (f) channels; S_1 and S_2 are particle spins; m_1 and m_2 (Z_1 and Z_2) are the masses (charges) of entrance-channel particles; K and J are, respectively, the wave number and the photon momentum in the exit channel; and I_J is the integral of the wave functions for the initial (χ_i) and final (χ_f) states (that is, the functions describing the relative motion of the clusters) with respect to the intercluster distance R. Sometimes, the spectroscopic factor S_{Jf} for the final state of the nucleus is included in the above expression for the cross sections but, in the potential cluster model used in this study, it is equal to unity, as was adopted in [5].

The results of our calculations show that the ^2S-wave scattering potential obtained above on the

Table 4. Variational parameters and coefficients in the expansion of the radial wave function for the ground bound state of the p^6Li system for the P-wave potential in (5) (the normalization factor for the function with these coefficients over the interval 0–25 fm is $N = 0.9999999999999895$)

i	β_i	C_i
1	2.477181344627947E-002	1.315463702527344E-003
2	5.874061769072439E-002	1.819913407984276E-002
3	1.277190608958812E-001	9.837541674753882E-002
4	2.556552559403827E-001	3.090018297080802E-001
5	6.962545656024610E-001	−1.195304944694753
6	87.215179556255360	3.237908749007494E-003
7	20.660304078047520	5.006096657700867E-003
8	1.037788131786810	−6.280751485496025E-001
9	2.768782138965186	1.282309968994793E-002
10	6.753591325944827	8.152343478073063E-003

Table 5. Variational parameters and coefficients in the expansion of the radial wave function for the first excited bound state of the p^6Li system for the P-wave potential in (6) (the normalization factor for the function with these coefficients over the interval 0–25 fm is $N = 0.9999999999999462$)

i	β_i	C_i
1	2.337027900191992E-002	1.218101547601343E-003
2	5.560733180673633E-002	1.653319276756672E-002
3	1.214721917930904E-001	9.009619752334307E-002
4	2.474544878067495E-001	3.003291466882630E-001
5	7.132725465249825E-001	−1.332325501226168
6	84.896023494945160	3.273725679869025E-003
7	1.162854732120233	−5.340018423135894E-001
8	1.574203000936825	9.367648737801053E-002
9	5.779896847077723	1.033713941440747E-002
10	19.422905786572090	5.314592946045428E-003

basis of the partial-wave analysis from [23] and characterized by the depth of 110 MeV underestimates strongly the astrophysical S factor. At the same time, the doublet ^2S-wave potential having a depth of 126 MeV and following from our partial-wave analysis describes correctly the behavior of the experimental S factor, as is shown in Fig. 6. The dashed curve in this figure represents the result for the transitions from the ^2S and ^2D scattering waves to the ground state of the ^{7}Be nucleus, the dotted curve represents the results for transitions to the first excited state, and the solid curve represents the total S factor. The displayed points (triangles and closed and open circles) stand for experimental data obtained in [38] (they are presented in [39]). The calculated $S_{1/2}$ factor (dotted curve) describes quite well experimental data for transitions to the first excited state of the ^{7}Be nucleus at low energies (open circles).

The $S(10)$ factor at 10 keV is $S_{3/2} = 76$ eV b and $S_{1/2} = 38$ eV b, its total value being 114 eV b. For the sake of comparison, we present known results for the total $S(0)$ factor from various studies. They are 79(18) [40], 105 (at 10 keV) [39], and 106 eV b [41]. The S-factor values presented in [42] are 39 eV b for transitions to the ground state and 26 eV b for the

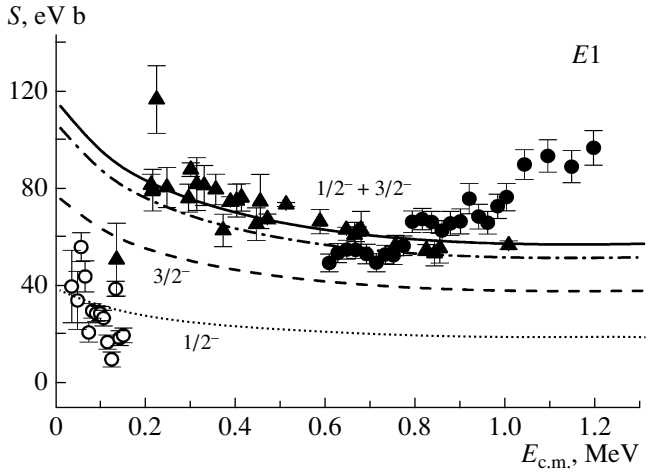

Fig. 6. Astrophysical S factor for the capture reaction $p^6\mathrm{Li} \to {}^7\mathrm{Be}\,\gamma$. The displayed points correspond to experimental data from [38] (they are presented in [39]). The dashed, dotted, solid, and dash-dotted curves represent, respectively, results for the transitions from the ${}^2S$ and ${}^2D$ scattering waves to the ground state of the ^{7}Be nucleus, results for transitions to the first excited state, the total S factor, and results of the calculations with a modified ${}^2S$-wave potential.

transition to the first excited state, so that the total S factor is 65 eV b. One can readily see that the scatter of these experimental data is rather large, and our results agree with them in general.

Additionally, a small change in the depth of the ${}^2S$-wave potential for p^6Li scattering has virtually no effect on the behavior of the calculated phase shifts, but it affects significantly the S factor at zero energy. If, for example, we set the potential depth to 124 MeV (the dotted curve in Fig. 5*a* represents the respective phase shifts), the S factor at the energy of 10 keV appears to be 105 eV b. In Fig. 6, the energy dependence of the total S factor calculated with the above potential is represented by the dash-dotted curve. Within the errors, this curve is compatible with experimental data at energies below 1 MeV.

It is noteworthy that, if we use potentials that do not involve forbidden states or those that involve a different number of forbidden states in the S or P waves, then the calculated S factor appears to be considerably smaller than the values obtained above. For example, the ${}^2S$-wave potential involving one forbidden state, having the parameters set to 25 MeV and 0.15 fm^{-2}, and providing a rather good description of phase shifts and the above ground-state potential yield an S-factor value of about 1 eV b at 10 keV.

CONCLUSIONS

The differential cross sections (angular distributions) for elastic ${}^6\mathrm{Li}(p,p){}^6\mathrm{Li}$ scattering were measured at the UKP-2-1 electrostatic tandem accelerator of the Institute of Nuclear Physics at the National Nuclear Center of the Republic of Kazakhstan (Almaty) at the energies of 593.0, 746.4, 866.8, 976.5, and 1136.3 keV in the angular range of 30–170°. The excitation functions were also measured over the energy range $E_p = 345$–1206 keV with a step of 50 keV at angles of 90° and 170° in the center-of-mass frame. The total error in the experimental data does not exceed 10%. These and some other data were analyzed on the basis of the optical model, and the result showed good agreement with experimental data, this favoring a purely potential mechanism of the formation of cross sections for elastic proton scattering on ^{6}Li nuclei.

In order to determine intercluster potentials on the basis of phase shifts, we thereupon performed a partial-wave analysis of the experimental data that were obtained here for elastic p^6Li scattering. On the basis of the resulting phase shifts for the elastic scattering of the clusters, we constructed continuous-spectrum intercluster-interaction potentials undergoing mixing in Young tableaux and involving forbidden states. Each partial wave was described by a respective Gaussian potential characterized by specific parameter values. In order to describe the bound state of the ^{7}Be nucleus, we used potentials that are pure in Young tableaux and which describe their basic features—first of all, the binding energy.

The classification of orbital states according to Young tableaux that was used in the present study makes it possible to determine the number of forbidden states and, hence, to fix almost unambiguously the depth of the potential that describes a certain partial-wave phase shift. The energy dependence of the phase shifts that was extracted from experimental data enabled an almost unambiguous determination

of the width of this potential. Thereby, the methods used here to obtain the shape and the depth of intercluster-interaction potentials permitted avoiding the discrete and continuous ambiguities marring the determination of their parameters within known versions of the optical model.

As a result, the doublet ^2S-wave phase shifts obtained in our partial-wave analysis, which takes explicitly into account the doublet ^2P wave, led to a potential that, in contrast to the potential constructed by using the results of the analysis performed in [23], allowed us to describe the experimental S factor at energies below 1 MeV. Thus, we have seen that, in just the same way as in the case of light nuclei [43, 44], the potential cluster model that employs the potentials proposed here makes it possible to obtain, in describing the astrophysical S factor for radiative proton capture by the ^{6}Li nucleus in the low-energy region, results that agree with data from known experiments.

ACKNOWLEDGMENTS

We are grateful to Yu.N. Uzikov (Joint Institute for Nuclear Research, Dubna) for enlightening discussions on some issues considered in the present study.

REFERENCES

1. *Essays in Nuclear Astrophysics*, Ed. by Ch. Barnes, D. Clayton, and D. Schramm (Cambridge Univ., Cambridge, 1982; Mir, Moscow, 1986).
2. O. F. Nemets, V. G. Neudatchin, A. T. Rudchik, Yu. F. Smirnov, and Yu. M. Tchuvil'sky, *Nucleon Clusterss in Nuclei and Multinucleon-Transfer Reactions* (Nauk. dumka, Kiev, 1988) [in Russian].
3. S. B. Dubovichenko, A. V. Dzhazairov-Kakhramanov, and A. A. Sakharuk, Yad. Fiz. **56** (8), 90 (1993) [Phys. At. Nucl. **56**, 1044 (1993)].
4. I. M. Kapitonov, B. S. Ishkhanov, and I. A. Tutyn', *Nucleosynthesis in the Universe* (Librokom, Moscow, 2009); http://nuclphys.sinp.msu.ru/nuclsynt.html
5. S. Angulo et al., Nucl. Phys. A **656**, 3 (1999).
6. V. G. Neudatchin, A. A. Sakharuk, and Yu. F. Smirnov, Fiz. Elem. Chastits At. Yadra **23**, 479 (1992) [Sov. J. Part. Nucl. **23**, 210 (1992)]; V. G. Neudatchin, B. G. Struzhko, and V. M. Lebedev, Fiz. Elem. Chastits At. Yadra **36**, 889 (2005) [Phys. Part. Nucl. **36**, 468 (2005)].
7. M. Skill et al., Nucl. Phys. A **581**, 93 (1995).
8. A. A. Arzumanov et al., in *Proceedings of the 13th Particle Accelerator Conference, Dubna, Russia, 13–15 Oct. 1992*, Vol. 1, p. 118; http://www.inp.kz/structure/ukp/_ukp.php?u=1#ac
9. J. W. Butler, NRL Report No. 5282, U.S. Naval Research Laboratory (1959).
10. P. B. Lyons, J. W. Toevs, and D. G. Sargood, Nucl. Phys. A **130**, 1 (1969).
11. M. K. Baktybayev et al., in *Proceedings of the 4th Eurasian Conference on Nuclear Science and its Application, Baku, Azerbaijan, Oct. 31–Nov. 3, 2006,* p. 147; Presentations, p. 418.
12. D. M. Zazulin, Vestn. NYaTs RK, No. 3, 22 (2007).
13. D. M. Zazulin, in *Proceedings of the 7th Intern. Conference on Nuclear and Radiation Physics, Almaty, Kazakhstan, 8–11 Sept., 2009,* p. 55.
14. O. F. Nemets and Yu. V. Gofman, *Handbook in Nuclear Physics* (Nauk. Dumka, Kiev, 1975) [in Russian].
15. J. A. McCray, Phys. Rev. **130**, 2034 (1963).
16. P. E. Hodgson, *Optical Model of Elastic Scattering* (Clarendon, Oxford, 1963; Atomizdat, Moscow, 1966).
17. F. G. Perey, *SPI-GENOA an Optical Model Code* (unpublished).
18. W. D. Harrison and A. B. Whitehead, Phys. Rev. **132**, 2607 (1963).
19. K. H. Bray et al., Nucl. Phys. A **189**, 35 (1972).
20. S. W. Chen and N. M. Hintz, in *Proceedings of the International Conference on Nuclear Physics* (Dunod, Paris, 1958), p. 387; *Nuclear Forces and the Few-Nucleon Problem*, Ed. by T. C. Griffith and E. A. Powers (Pergamon, Oxford, 1960), p. 683.
21. C. M. Perey and F. G. Perey, At. Data Nucl. Data Tables **17**, 2 (1976).
22. R. Barrett and D. Jackson, *Nuclear Size and Structure* (Clarendon, New York, 1977; Nauk. Dumka, Kiev, 1981).
23. C. Petitjean, L. Brown, and R. G. Seyler, Nucl. Phys. A **129**, 209 (1969).
24. S. B. Dubovichenko, Yad. Fiz. **71**, 66 (2008) [Phys. At. Nucl. **71**, 65 (2008)].
25. http://physics.nist.gov/cgi-bin/cuu/Value?mud|search_for=atomnuc!
26. S. B. Dubovichenko, *Methods for Calculating Nuclear Properties* (Kompleks, Almaty, 2006) [in Russian].
27. V. G. Neudatchin and Yu. F. Smirnov, *Nucleon Clusters in Light Nuclei* (Nauka, Moscow, 1969) [in Russian].
28. C. Itzykson and M. Nauenberg, Rev. Mod. Phys. **38**, 95 (1966).
29. A. Bohr and B. Mottelson, *Nuclear Structure*, vol. 1: *Single-Particle Motion* (Benjamin, New York, 1975; Mir, Moscow, 1977).
30. S. B. Dubovichenko, Yad. Fiz. **73**, 1573 (2010) [Phys. At. Nucl. **73**, 1526 (2010)].
31. S. B. Dubovichenko and A. V. Dzhazairov-Kakhramanov, Fiz. Elem. Chastits At. Yadra **28**, 1529 (1997) [Phys. Part. Nucl. **28**, 615 (1997)].
32. S. B. Dubovichenko, *Properties of Light Nuclei in the Potential Cluster Model* (Daneker, Almaty, 2004) [in Russian].
33. D. R. Tilley et al., Nucl. Phys. A **708**, 3 (2002).
34. S. B. Dubovichenko, Izv. NAN RK, Ser. Fiz.-Mat., No. 4, 49, 52 (2007).

35. W. A. Fowler, G. R. Caughlan, and B. A. Zimmerman, Ann. Rev. Astron. Astrophys. **13**, 69 (1975).
36. E. E. Salpeter, Phys. Rev. **88**, 547 (1952).
37. http://physics.nist.gov/cgi-bin/cuu/Value?hbar|search_for=universal_in!
38. Z. E. Switkowski et al., Nucl. Phys. A **331**, 50 (1979); R. Bruss et al., in *Proceedings of the 2nd International Symposium on Nuclear Astrophysics, Nuclei in the Cosmos, Karlsruhe, Germany, 6–10 Jul., 1992*, Ed. by F. Kappeler and K. Wisshak (IOP Publ., Bristol, England, 1993), p. 169.
39. K. Arai, D. Baye, and P. Descouvemont, Nucl. Phys. A **699**, 963 (2002).
40. R. M. Prior et al., Phys. Rev. C **70**, 055801 (2004).
41. F. C. Barker, Austr. J. Phys. **33**, 159 (1980).
42. F. E. Cecil et al., Nucl. Phys. A **539**, 75 (1992).
43. S. B. Dubovichenko, Izv. Vyssh. Uchebn. Zaved., Ser. Fiz. **52** (3), 68 (2009); S. B. Dubovichenko and A. V. Dzhazairov-Kakhramanov, Eur. Phys. J. A **39**, 139 (2009).
44. S. B. Dubovichenko, N. Zh. Takibaev, and L. M. Chechin, *Physical Processes in Far and Near Space* (Daik-Press, Almaty, 2008) [in Russian].

Translated by A. Isaakyan